Magnetically induced ferroelectricity in the buckled Kagome antiferromagnet $Ni_3V_2O_8$

2008 J. Phys.: Condens. Matter 20 434205

(http://iopscience.iop.org/0953-8984/20/43/434205)

J. Phys.: Condens. Matter **20** (2008) 434205 (9pp) doi:10.1088/0953-8984/20/43/434205

Magnetically induced ferroelectricity in the buckled Kagome antiferromagnet $Ni_3V_2O_8$

G Lawes[1], M Kenzelmann[2,3] and C Broholm[4,5]

[1] Department of Physics and Astronomy, Wayne State University, Detroit, MI 48201, USA
[2] Laboratory for Solid State Physics, ETH Zurich, CH-8093 Zurich, Switzerland
[3] Laboratory for Neutron Scattering, ETH Zurich and Paul Scherrer Institute, CH-5232 Villigen, Switzerland
[4] Department of Physics and Astronomy, Johns Hopkins University, Baltimore, MD 21218, USA
[5] NIST Center for Neutron Research, National Institute of Standards and Technology, Gaithersburg, MD 20899, USA

Received 29 February 2008, in final form 21 April 2008
Published 9 October 2008
Online at stacks.iop.org/JPhysCM/20/434205

Abstract

$Ni_3V_2O_8$ is one of several recently identified multiferroic materials in which ferroelectricity is produced by long-range magnetic order. This staircase Kagome compound adopts a sequence of distinct low temperature magnetic phases, which exhibit different optical, dielectric, and transport properties, most notably ferroelectric order arising from a polar incommensurate magnetic structure. We give an overview of the experimental results from the existing literature on $Ni_3V_2O_8$, and briefly discuss models that describe the coupling between magnetic and ferroelectric properties. We show that the temperature dependence of the dielectric constant provides evidence for spin–charge coupling in $Ni_3V_2O_8$ away from the ferroelectric phase. An anomaly in the thermal conductivity at the incommensurate–commensurate phase transition suggests that spin scattering may limit thermal transport in the incommensurate phase. We associate each of the two incommensurate phase transitions with one magnetic order parameter, and we show that the temperature dependence of the ferroelectric polarization closely follows the product of these two magnetic order parameters—corroborating the validity of the phenomenological trilinear coupling model. Finally, we present inelastic powder neutron scattering measurements that provide evidence of several weakly dispersive magnetic modes that are typical for strongly frustrated antiferromagnets with large spin anisotropies.

1. Introduction

Many of the new functionalities envisioned for next generation electronic devices, most notably the electric field control of spin and other magnetic properties, require the development of entirely new materials that exhibit a variety of strongly coupled microscopic or macroscopic properties [1–3]. Some of the applications envisioned for these novel devices include voltage switchable magnetic memory [4, 5] and electric field tuning of spin polarized currents [6]. Magnetoelectric multiferroic materials, which express simultaneous magnetic and ferroelectric order that are strongly coupled, are particularly attractive for these types of applications. While a handful of multiferroic materials had been identified by the turn of the century [3, 7–9], it was recognized that the characteristics typically responsible for driving magnetism, namely unpaired electrons in d orbitals, were inimical to a conventional requirement for producing ferroelectric order, namely a d^0 electronic structure [10]. However, over the past several years, there has been considerable interest in investigating materials in which the multiferroic behavior arises through atypical mechanisms, including ferroelectric order promoted by magnetic order [11–13], and structural effects in both homogeneous and heterogeneous systems [14, 15]. While some of these materials are not immediately useful for device applications, this research has

led to a deeper understanding of the physical mechanisms underlying the development of multiferroic properties. Within this broader framework, we discuss some of the principle experimental results concerning the development of magnetic and ferroelectric order in one specific multiferroic oxide, $Ni_3V_2O_8$ [12]. This geometrically frustrated magnet adopts a number of different magnetic structures at low temperatures [16], one of which creates a polar axis and leads to ferroelectricity. In this context, $Ni_3V_2O_8$ is a particularly simple model system for investigating magnetically induced ferroelectric order in atypical multiferroic materials [4, 17].

The magnetic characteristics of $Ni_3V_2O_8$ descend from the arrangement of Ni^{2+} ions on buckled Kagome lattices, which are stacked along the **b** axis. The system crystallizes in the orthorhombic space group *Cmca* and is structurally anisotropic, with room temperature lattice parameters of $a = 5.92$ Å, $b = 11.37$ Å, and $c = 8.22$ Å, although there are significant distortions associated with the low temperature magnetic phase transitions [18]. While topologically equivalent to conventional Kagome lattices, the *staircase* Kagome structure of $Ni_3V_2O_8$ breaks the symmetry of the pure Kagome web by introducing alternating bends along the **c** axis. This results in the development of two inequivalent Ni^{2+} sites, which we will refer to as *spine* and *cross-tie* sites. The broken Kagome symmetry leads to a number of inequivalent magnetic interactions, most notably symmetric next nearest-neighbor and anisotropic Dzyaloshinskii–Moriya (DM) interactions, and to strong spin anisotropy with an easy axis along the **a** axis [16]. The crystal structure for $Ni_3V_2O_8$ is illustrated in figure 1, which shows the crystal structure with views nearly along the **b** and **a** axes, respectively. The spine sites form chains along the **a** axis, consisting of slightly staggered oxygen octahedra with a Ni^{2+} at the center. The crystal structure is buckled, leading to two different locations of theses chains along the **b** axis. There are oxygen tetrahedra with non-magnetic V^{5+} ions in the center that are attached to the oxygen octahedra. The figure also shows that the crystal structure allows for sizeable magnetic interactions between the buckled Kagome planes.

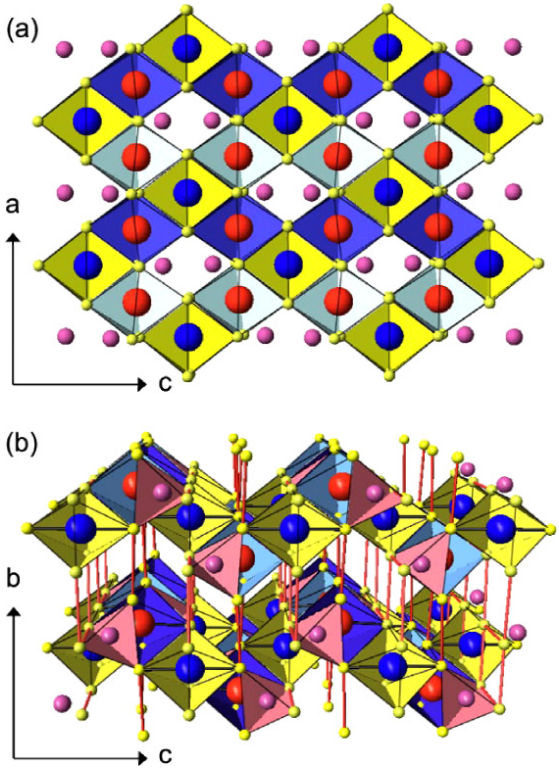

Figure 1. $Ni_3V_2O_8$ crystal structure viewed (a) along nearly the **b** axis and (b) along nearly the **a** axis. The spine Ni^{2+} sites are shown in red, the cross-tie Ni^{2+} sites are shown in blue and the V^{5+} are shown in pink. Also shown are the oxygen octahedra of the spine sites in light and dark blue, and those of the spine sites in yellow. The oxygen tetrahedra around the V^{5+} are shown in pink. Also shown as red solid lines in (b) are the possible superexchange pathways along the **b** axis between Ni^{2+}.

2. Synthesis

Polycrystalline $Ni_3V_2O_8$ can be synthesized using a number of standard solid-state techniques for producing oxide materials. However, because of the anisotropic magnetic and ferroelectric properties of this material, it is highly desirable to study single crystal samples. High quality singly crystal $Ni_3V_2O_8$ samples can be grown from a $BaO–V_2O_5$ flux [16]. The $Ni_3V_2O_8$ crystals prepared through this technique typically consist of large platelets, having an area of up to several cm^2 with a thickness of approximately 0.1 cm. These $Ni_3V_2O_8$ crystals grow with the **b** axis perpendicular to the large face of the crystal, making dielectric and ferroelectric measurements along the **b** axis straightforward for the as-prepared samples. $Ni_3V_2O_8$ single crystals can also be prepared using a floating zone technique in an optical furnace [19]. The single crystal samples prepared using this technique are quite large, having a diameter of roughly 0.8 cm and a length of well over 7 cm, and are suitable for studies that require detailed measurements of the physical properties of $Ni_3V_2O_8$ along all three principle crystallographic directions.

3. $Ni_3V_2O_8$ field-temperature phase diagram

The phase diagram of $Ni_3V_2O_8$ as a function of magnetic field (H) and temperature (T) has been determined through thermodynamic, magnetic, dielectric, ferroelectric, optical, and other measurements [12, 16, 18, 20–22]. This phase diagram for magnetic fields along the **a** and **c** axes is plotted in figure 2. At temperatures above approximately 12 K, $Ni_3V_2O_8$ is purely paramagnetic (P), with no magnetic or electric long-range order. Short-range magnetic correlations develop with decreasing temperature, with the onset of zero-field long-range magnetic order at $T_H = 9.2$ K. Neutron measurements, discussed in detail in section 7.2, establish that this spin structure has incommensurate modulation along the **a** axis [16, 20]. We will refer to this as the high temperature incommensurate phase (HTI). At $T_L = 6.4$ K there is a magnetic transition to another incommensurately modulated magnetic structure, which we will refer to as the low temperature incommensurate (LTI) phase. At $T_C = 4.2$ K $Ni_3V_2O_8$ undergoes a first order phase transition to

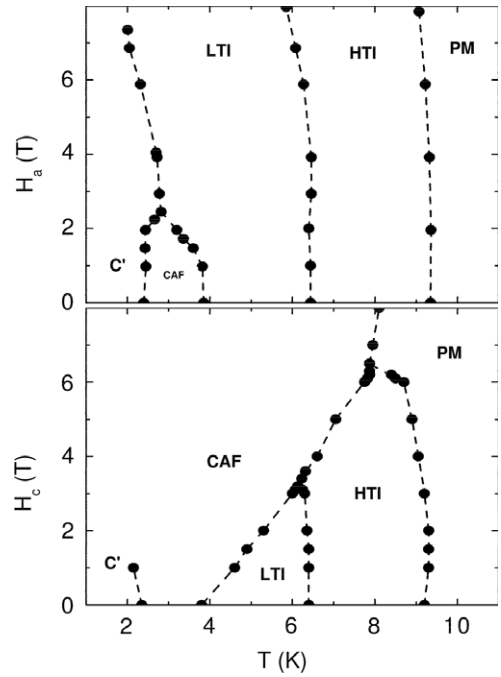

Figure 2. (a) Phase diagram for $Ni_3V_2O_8$ determined for the magnetic field H applied along the **a** axis. (b) Phase diagram for H along **c**. For both panels, the data points were determined using specific heat measurements and the dashed lines are intended as a guide-to-the-eye.

a canted antiferromagnetic (CAF) phase, in which the spins are ordered antiferromagnetically along the **a** axis, with a small spin canting along the **c** axis. There is one additional zero-field magnetic transition occurring at $T_{C'} = 2.5$ K, although the magnetic structure of $Ni_3V_2O_8$ in this ground state (C′) has yet to be determined. The most significant feature of the phase diagram is the observation that the LTI phase exhibits ferroelectric order, as demonstrated by a spontaneous polarization along the **b** axis [12]. The fact that $Ni_3V_2O_8$ develops ferroelectric order in only one of the distinctly different magnetic phases is a stringent restriction for the development of a model for magnetically induced ferroelectricity in this multiferroic system [4, 12, 17].

The H–T phase diagram of $Ni_3V_2O_8$ depends strongly on the direction of the applied magnetic field, reflecting its anisotropic magnetic properties. In all cases, the P–HTI and HTI–LTI phase boundaries are relatively insensitive to small applied magnetic fields. These phase boundaries are nearly constant in temperature as a function of magnetic field, exhibiting shifts of less than 0.2 K in fields up to several Tesla. Applying a magnetic field along the **c** axis favors the CAF phase, as can be seen in figure 2(b), while the application of a magnetic field along **a** suppresses the CAF phase and promotes the LTI phase (figure 2(a)). There remains some ambiguity concerning the low temperature phase of $Ni_3V_2O_8$ in an applied magnetic field. Specific heat measurements suggest the system remains in the C′ phase [16], while spontaneous polarization measurements hint that there could be another phase developing above an applied field of 2 T applied along the **a** axis [12]. Recent magnetic measurements also give evidence for an additional low temperature phase above this 2 T threshold field [22], which strongly argues that there is a field induced phase transition in $Ni_3V_2O_8$ at low temperatures. High field optical measurements on $Ni_3V_2O_8$ [21] indicate additional phase transitions, suggesting the existence of another phase of $Ni_3V_2O_8$, which develops above magnetic fields of roughly $\mu_0 H = 10$ T applied along the **b** axis. Magnetization measurements also show evidence for a high field phase developing in magnetic fields above approximately $\mu_0 H = 8$ T applied along the **a** axis [22].

There are specific structural changes associated with the magnetic transitions in $Ni_3V_2O_8$. The LTI phase is ferroelectric, and the presence of electric dipoles is necessarily associated with a structural distortion. However, given the very small magnitude of the ferroelectric polarization, on the order of only 100 $\mu C\,m^{-2}$ [12], the structural modifications associated with ferroelectric order are also expected to be very small and they have not yet been observed microscopically. Based on a specific model for spin–phonon mediated interactions, the oxygen displacement associated with ferroelectricity is expected to be only on the order of 0.0005 Å [17]. More significant structural changes are observed at the LTI–CAF phase transition through direct measurements of the lattice strain. There is significant anisotropy in the thermal expansion of $Ni_3V_2O_8$ at the CAF transition, with the **a** and **b** axes expanding, by $\Delta a/a = 1.65 \times 10^{-5}$ and $\Delta b/b = 3.97 \times 10^{-5}$ respectively, and the **c** axis showing a contraction of $\Delta c/c = -8.24 \times 10^{-5}$ [18]. This magnetostriction leads to a relatively small reduction in volume on the transition to the CAF phase.

4. Models for $Ni_3V_2O_8$

The fascinating sequence of magnetic structures exhibited by $Ni_3V_2O_8$ results from the interplay of the inequivalent interactions from spine Ni^{2+} ions on the buckled Kagome lattice. The spin structures are the result of competing isotropic nearest-neighbor (NN) and second nearest-neighbor (SNN) interactions, together with the anisotropic DM interaction and easy axis anisotropy [4, 16, 17]. In the presence of easy axis anisotropy and sufficiently large SNN interactions, the theoretically predicted phase is a longitudinally modulated phase with the spins confined to the easy (**a**) axis [23], consistent with the results of neutron studies of the HTI phase in $Ni_3V_2O_8$. An additional transverse modulated component is expected as the temperature is further reduced, corresponding to the LTI phase. The weak ferromagnetic moment in the CAF phase can arise from DM interactions between the spine and cross-tie spins, and a pseudodipolar interaction between the spine and cross-tie spins. More complete discussions on the models used to describe the magnetic phase in $Ni_3V_2O_8$ can be found in [4, 16, 20].

One of the most striking features of $Ni_3V_2O_8$ is the development of ferroelectric order in the LTI magnetic structure. $Ni_3V_2O_8$ exhibits a smoothly increasing spontaneous polarization below T_L, which vanishes abruptly at the transition to the CAF phase [12]. This polarization arises only along the **b**

axis, and the development of ferroelectric order can be understood using a model with a trilinear coupling between the ferroelectric order parameter (P), the HTI magnetic order parameter ($\sigma_{\rm HTI}$), and the LTI magnetic order parameter ($\sigma_{\rm LTI}$) [12]. Within this framework, and based on a mean field approximation, the only non-zero component of the polarization is given by $P_{\rm b} = C\chi_{\rm el}\sigma_{\rm HTI}\sigma_{\rm LTI}$, with C a constant and $\chi_{\rm el}$ the electric susceptibility. Spin–phonon interactions have been proposed as a possible mechanism giving rise to the coupling between magnetic and ferroelectric order in $Ni_3V_2O_8$, either via DM interactions or strain derivatives of the exchange tensors [17].

5. Thermodynamic properties

The cascade of phase transitions that define the magnetic and ferroelectric properties of $Ni_3V_2O_8$ at low temperatures are most directly observable through thermodynamic measurements [16]. The zero-field $Ni_3V_2O_8$ specific heat, plotted as C/T versus T in figure 3(a), shows distinct peaks at $T = 9.2$ and 6.4 K corresponding to second order phase transitions into incommensurate magnetically ordered states. There is a very large peak associated with a first order magnetic phase transition at $T = 4.2$ K, and a fourth, small second order peak at $T = 2.5$ K. These specific heat peaks are superimposed on top of a large background heat capacity of approximately $C/T = 0.7$ J/mole$_{\rm Ni}$ K^2. This large background develops below approximately 10 K, and persists down to low temperatures. Such behavior is characteristic for low-dimensional and geometrically frustrated magnets and is associated with the development of short-range magnetic correlations in the paramagnetic state and with the presence of low lying magnetic excitations in the ordered state [24]. For $Ni_3V_2O_8$ the entropy difference between 0 and 30K was estimated as 7.6 J/mole$_{\rm Ni}$ K [25]. This value is not far from the total entropy associated with one mol of completely disordered spin-1, so the magnetic ground state of $Ni_3V_2O_8$ may retain 16% of the R ln(3) entropy expected for a spin-1 system.

Figure 3(b) shows the thermal conductivity of $Ni_3V_2O_8$ measured along the **b** axis as a function of temperature at zero magnetic field. While there are no obvious anomalies in thermal conductivity associated with either the HTI or LTI magnetic transitions, there is a clear feature at the CAF transition temperature. This feature is indicated with an arrow in figure 3(b). There is also some small scatter in the thermal conductivity data close to $T = 7$ K, which we attribute to noise in the measurement. Just above $T_{\rm C}$, the thermal conductivity varies approximately like $T^{1.8}$, as shown by the solid line in figure 3(b). While this deviates somewhat from the T^2 temperature dependence expected for phonon-defect scattering [26] (shown in figure 3(b) as a dashed line), we believe that the thermal conductivity between $T_{\rm C}$ and $T \approx 10$ K is heavily influenced by phonon scattering from defects. It has been suggested that phonon scattering from spin fluctuations may affect the thermal conductivity in frustrated magnets [27]; a similar mechanism could be partially responsible for the temperature dependence of the thermal conductivity in $Ni_3V_2O_8$. The thermal conductivity increases slightly in the CAF phase, which could indicate a reduction of scattering from spin fluctuations in this commensurately ordered phase, but might also signal the onset of new mechanisms for thermal conduction.

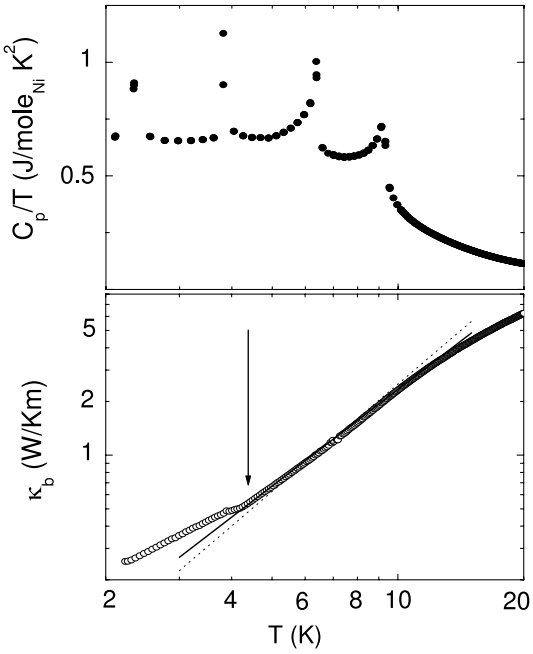

Figure 3. (a) Temperature dependent specific heat of $Ni_3V_2O_8$ measured at $H = 0$ and plotted as C/T versus T. (b) Temperature dependent thermal conductivity of $Ni_3V_2O_8$ measured along the **b** axis at $H = 0$. The arrow indicates $T_{\rm C}$, the solid line illustrates a $T^{1.8}$ dependence, and the dashed line shows a T^2 dependence, as described in the text.

6. Ferroelectric properties

6.1. Dielectric constant

The onset of ferroelectric order in $Ni_3V_2O_8$ leads to a large dielectric anomaly at $T_{\rm L}$. The dielectric constant of $Ni_3V_2O_8$ shows an increase of between 15% and 20%, for measuring frequencies between $\omega/2\pi = 3$ and 300 kHz, centered at the transition temperature, as shown in figure 4(a). The fact that the magnitude of this dielectric response increases as the measuring frequency is reduced from 300 to 3 kHz points to the existence of some relatively slow dynamics at the transition. Because this frequency is much lower than for typical intrinsic timescales for microscopic processes, we believe this frequency dependence of the dielectric constant may be associated with the formation of multiferroic domains at the LTI phase transition.

Two other dielectric anomalies observed in $Ni_3V_2O_8$ can be associated with the development of magnetic order. The dielectric constant shows a sharp decrease, on the order of 5%, at the transition to the CAF phase. This is consistent with observations of magnetodielectric coupling in other systems with weak ferromagnetic order, where the onset of magnetic order can lead to a hardening of optical phonon modes and a corresponding decrease in dielectric constant [28]. A much smaller feature in the dielectric constant can be seen at the

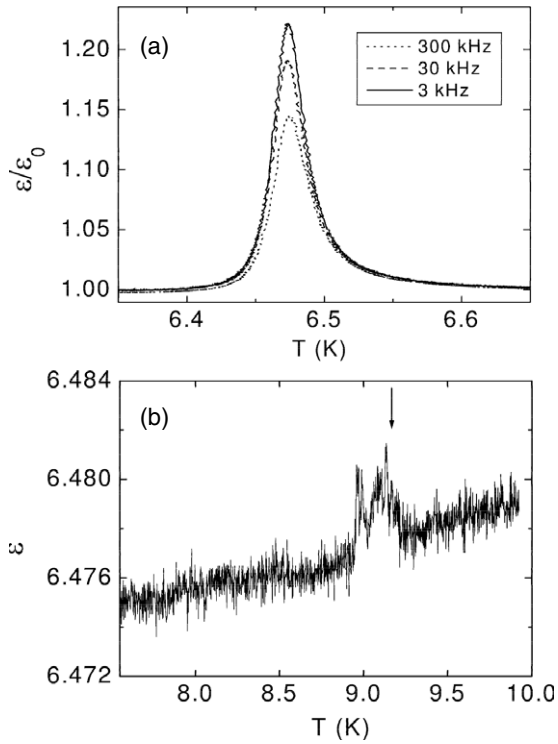

Figure 4. (a) Temperature dependent dielectric constant of $Ni_3V_2O_8$ measured at zero magnetic field at frequencies of $\omega/2\pi = 300$ kHz (lower curve), $\omega = 30$ kHz (middle curve), and $\omega/2\pi = 3$ kHz (upper curve). (b) Dielectric constant for $Ni_3V_2O_8$ measured at $H = 0$ for a small range of temperatures close to T_{HL}, which is indicated by an arrow.

onset of magnetic order in $Ni_3V_2O_8$ at $T_H = 9.2$ K. This very small anomaly has a magnitude of less than 0.1%, but can be seen in high-resolution dielectric measurements, as shown in figure 4(b). For some other $Ni_3V_2O_8$ samples, this very small feature can only be observed after subtracting a background contribution to the dielectric constant. The physics of this anomaly is discussed briefly in [29]. This result is significant, because it demonstrates that $Ni_3V_2O_8$ features distinct changes of the spin–charge coupling outside of the ferroelectric phase.

6.2. Ferroelectric measurements

The spontaneous polarization of $Ni_3V_2O_8$ was determined by measuring the pyrocurrent. For these measurements, the $Ni_3V_2O_8$ crystal is poled by applying a substantial ($\approx$2 kV cm^{-1}) voltage across the sample while cooling through the ferroelectric transition, removing this bias at base temperature, and then measuring the current, which is proportional to $\frac{dP}{dt}$ upon heating through T_C. The polarization P is determined by integrating this pyrocurrent. It is found that the direction of the spontaneous polarization depends on the sign of the poling voltage [12], as expected for ferroelectrics. One interesting point to note is that the base temperature for ferroelectric measurements in $Ni_3V_2O_8$ can be below T_C. The CAF phase does not exhibit ferroelectric order, but nevertheless can be imprinted by the poling bias. This may be caused by local regions with LTI magnetic structure that remain present in the CAF phase due to the first order phase transition between the LTI to CAF phases. LTI magnetic correlations can be seen at low temperatures using neutron scattering, but they can be suppressed by magnetic annealing [20, 30]. The spontaneous polarization in $Ni_3V_2O_8$ is rather small, reaching only 100 μC m^{-2} at zero field [12]. This increases to almost 150 μC m^{-2} with a magnetic field applied along the **a** axis, but is strongly suppressed by a magnetic field applied along **c**. As applying an external magnetic field along **a** can promote the development of ferroelectric order, the magnetoelectric coupling parameter $\alpha = \frac{dP}{dH}$ reaches over 0.06 μC m^{-2} Oe close to the critical field.

6.3. Optical characterization

The optical response of $Ni_3V_2O_8$ has been studied in great detail as a function of temperature and magnetic field [21]. The optical spectra show features corresponding to Ni d–d excitations at 0.75 and 1.35 eV, associated with the cross-tie and spine spins, respectively. A small splitting of the cross-tie peak indicates that the low temperature magnetic transitions in $Ni_3V_2O_8$ may be heralded by a subtle local structural distortion. The optical response of $Ni_3V_2O_8$ is also dramatically affected by an external magnetic field at low temperatures. The high energy dielectric constant shows shifts up to 15% at magnetic fields of $\mu_0 H = 30$ T near the spine spin d–d excitation feature, demonstrating that the strong magnetodielectric coupling observed at low frequencies persists into the optical regime.

7. Magnetic properties

7.1. Magnetization

The dominant magnetic interactions in $Ni_3V_2O_8$ are antiferromagnetic, as indicated by a Curie–Weiss temperature of $\theta_W = -30$ K [25]. $Ni_3V_2O_8$ shows long-range magnetic order only below $T_H = 9.2$ K, corresponding to a relatively small frustration index $f = \Theta_{CW}/T_{HL} = 3.2$. Despite magnetic ordering transitions at $T_H = 9.2$ K and $T_L = 6.4$ K, the temperature dependent magnetization of $Ni_3V_2O_8$ shows no significant features at these transitions [16]. $Ni_3V_2O_8$ does, however, show large and anisotropic magnetic anomalies associated at the LTI–CAF phase transition. The magnetization along the **c** axis shows a dramatic increase as $Ni_3V_2O_8$ is cooled below $T_C = 4.2$ K, while the magnetization along the **b** axis is almost constant and the magnetization measured along the **a** axis exhibits a distinct drop. These observations are consistent with the moments having antiferromagnetic order along the **a** axis with some small ferromagnetic moment arising from spin canting along the **c** axis. The magnetization shows thermal hysteresis at this first order phase transition, with a shift of approximately 0.02 K observed between measurements on warming and cooling at a time-average rate of less than 0.05 K min^{-1}. There is no clear magnetic anomaly associated with the transition into the C′ phase, making three out of the four magnetic phase transitions in $Ni_3V_2O_8$ difficult to discern using only bulk magnetization measurements.

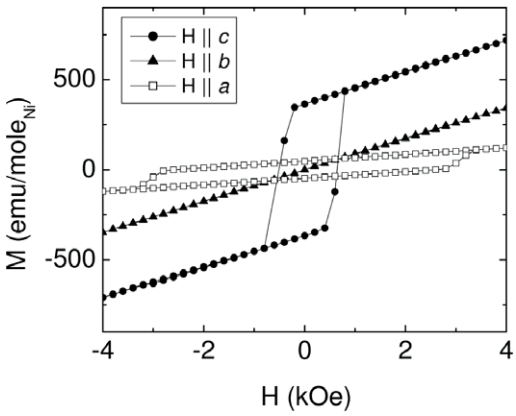

Figure 5. Magnetic hysteresis loops for $Ni_3V_2O_8$ with H applied along the **a** (open squares), **b** (closed triangles), and **c** (closed circles) axes measured at $T = 2$ K.

The strong magnetic anisotropy associated with the canted antiferromagnetic phase can also be seen in low temperature hysteresis measurements. We plot $M(H)$ loops for $Ni_3V_2O_8$ measured at $T = 2$ K in figure 5. When measured along the **b** axis, the magnetization is simply paramagnetic, exhibiting linear behavior with no hysteresis. The magnetization measured along the **a** axis shows a very broad hysteresis loop, with a coercive field of approximately 3 kOe, but having a net moment much smaller than that measured along the **b** axis away from $H = 0$ T. Conversely, the magnetic hysteresis loop measured parallel to the **c** axis shows a much smaller coercive field, only 1 kOe, but a substantially larger magnetization than along the other two crystallographic axes. At higher magnetic fields, the slope of the magnetization curves for H applied along the **b** and **c** axes are the same. This suggests that, neglecting the component of the spins associated with the spontaneous weak ferromagnetism in $Ni_3V_2O_8$, the **a** axis is an approximate uniaxial symmetry direction for the magnetic anisotropy.

7.2. Neutron measurements

Neutron diffraction measurements were used to determine the magnetic structure of $Ni_3V_2O_8$ as a function of temperature and field [16, 20]. At zero field, neutron scattering revealed that $Ni_3V_2O_8$ undergoes a transition to incommensurate magnetic order at $T_{HL} = 9.2$ K, described by an ordering wavevector $\mathbf{Q} = (q, 0, 0)$, where q indicates the temperature dependent modulation along the **a** axis. The temperature dependence of the magnetic Bragg peaks, shown in figure 6(a), provides clear evidence of an additional magnetic transition at $T_{HL} = 6.4$ K where $Ni_3V_2O_8$ becomes ferroelectric. At temperatures near

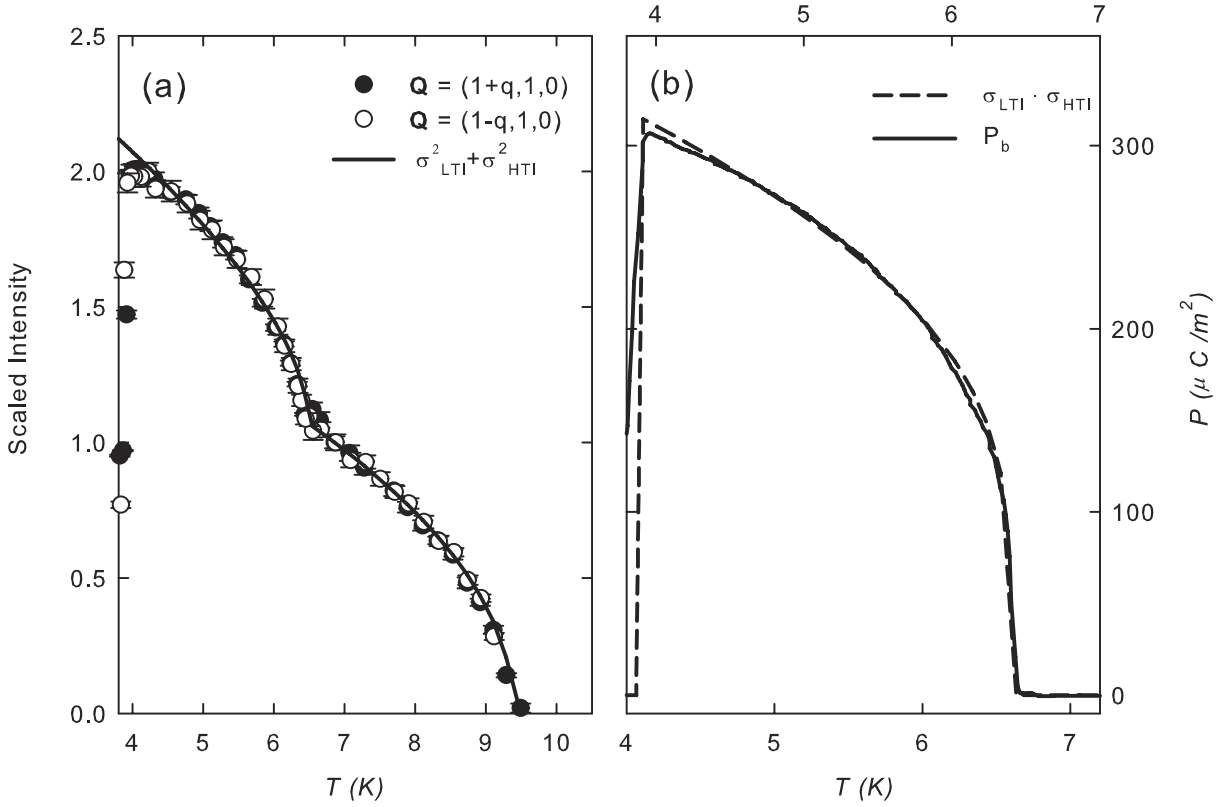

Figure 6. (a) Neutron scattering intensity for two incommensurate satellite peaks as a function of temperature, for $T_{HL} < T < T_{PH}$ scaled as $I(T)/I(T_{HL})$ and for $T_{LC} < T < T_{HL}$ scaled as $[I(T) - I(T_{HL})]/I(T_{LC}) + I(T_{HL})$. The solid line represents $\sigma^2_{LTI} + \sigma^2_{HTI}$, assuming that $\sigma_{LTI} \propto (T - T_{HL})^{\beta}$ and $\sigma_{HTI} \propto (T - T_{PH})^{\beta}$ with $\beta \sim 0.25$ (the data are however not of sufficient quality to determine critical exponents). (b) Temperature dependence of the electric polarization, as determined form pyroelectric measurements, compared to the product of the two magnetic order parameter $\sigma_{LTI}\sigma_{HTI}$. An arbitrary scale factor was adjusted to put the curve on top of the data. The data are shown using slightly shifted temperatures scales for these two independent measurements (bottom and top temperature scales refer to the electric and neutron measurements, respectively).

T_{HL} the incommensurate modulation q reverses its temperature dependence. The modulation indicated by q approaches a roughly constant value as the temperature approaches $T_{LC} = 4$ K where the incommensurate order gives way towards the onset to commensurate order.

The symmetry of the magnetic structure was determined in the paraelectric phase HTI at $T = 7$ K and in the ferroelectric LTI phase at $T = 5$ K. In the HTI phase, the magnetic structure is amplitude modulated along the **a** axis with the magnetic moments on the spine and cross-tie sites along the **a** and **b** axis, respectively. The temperature dependence of the magnetic Bragg peak intensity in the HTI phase normalized to the intensity at T_{HL}, $I(T)/I(T_{HL})$, is identical for two different magnetic Bragg peaks. This shows that the magnetic order in the HTI phase can be parameterized by a single magnetic order parameter σ_{HTI} as shown in figure 6(a). In the LTI phase, the magnetic structure is a cycloidal spiral modulated along the **a** axis and with rotating moments in the ab plane. Figure 6(a) shows that for $T_{LC} < T < T_{HL}$, the temperature dependence of the magnetic Bragg peaks intensity, scaled as $[I(T) - I(T_{HL})]/I(T_{LC}) + I(T_{HL})$, is identical for two magnetic Bragg peaks. This shows that the LTI phase can be described by σ_{HTI} and one additional magnetic order parameter σ_{LTI}. Finally, in the commensurate phase below T_{LC}, the magnetic structure consists of an anti-parallel arrangements of nearest-neighbor spin sites along the **a**-axis.

These neutron scattering measurements provide direct evidence that the ferroelectric polarization in $Ni_3V_2O_8$ is induced by long-range magnetic order. Within a mean field description, the trilinear coupling of electric and incommensurate magnetic order parameters gives rise to an electric polarization that is proportional to the product of the symmetry breaking magnetic order parameters, which is $\sigma_{HTI} \cdot \sigma_{LTI}$ for $Ni_3V_2O_8$ [16, 31]. Details of the symmetry properties of the magnetic order parameters in $Ni_3V_2O_8$ for $T > 2.3$ K can be found in [20]. Figure 6(b) shows that the temperature dependence of the ferroelectric polarization and of the product $\sigma_{LTI} \cdot \sigma_{HTI}$ are identical, providing a clear and unambiguous confirmation that ferroelectricity in $Ni_3V_2O_8$ is induced by magnetism through the proposed trilinear coupling term.

We explored the excitation spectrum of $Ni_3V_2O_8$ using inelastic neutron spectroscopy on a powder sample. The ideal two-dimensional Kagome lattice is an example of a heavily frustrated material with a low energy manifold of states. To lowest order in spin wave theory, the excitation spectrum contains zero-energy modes [32]. The inequivalence of nearest-neighbor interactions, next nearest exchange paths and spin anisotropy is likely to break the degeneracy of the ground state, favoring some over others, lifting degeneracies and shifting putative zero-energy modes to finite energies. They also leads to the succession of the long-range ordered magnetic structures observed for $Ni_3V_2O_8$, each with their distinct excitation spectra.

We determined the powder averaged imaginary component of the dynamic magnetic susceptibility, $\chi''(Q, \omega)$ multiplied by the form factor square of Ni^{2+} from time-of-flight measurements performed using the DCS spectrometer at NIST. We determined the dynamic structure factor $S(\mathbf{Q}, \omega)$ on an absolute scale, and used the following equation to determine $\chi''(Q, \omega)$ on an absolute scale:

$$S(Q, \omega) = \frac{1}{1 - \exp(-\beta\hbar\omega)} \frac{\chi''(Q, \omega)}{\pi(g\mu_B)^2}. \quad (1)$$

The results for $\chi''(Q, \omega)$ are shown in figure 7 for two energy windows and two temperatures. At $T = 30$ K, the magnetic susceptibility does not contain any sharp features. The maxima in intensity at around $Q = 0.4$ and 1.6 Å^{-1} indicate short-range spin correlations. The dynamic magnetic susceptibility extends to about 4.5 meV. Because a powder inelastic measurements integrates over all magnetic excitations, this upper energy cutoff suggests that the most energetic magnetic excitations are at around 4.5 meV—an energy scale that is not too far from the Curie–Weiss temperature.

The dynamic magnetic susceptibility changes qualitatively upon cooling to $T = 1.5$ K, where $\chi''(Q, \omega)$ features several well-defined modes. This is remarkable, as it is usually not possible to discern such clear magnetic features in a powder averaged neutron spectrum. The data indicate that there exist very weakly dispersive excitations in $Ni_3V_2O_8$. The weak dispersion of the modes suggest that they are associated with local excitations, and that they are possibly related to the zero-energy excitations of the Heisenberg Kagome model. Previous inelastic neutron measurements using a single crystal along the $[h, 3, 0]$ reciprocal direction are consistent with our results, identifying at least two magnetic excitation branches below 4.5 meV: a low energy branch with a strong spectral weight around 1 meV and a higher energy branch with a much weaker spectral weight around 3.5 meV [33]. More single crystal inelastic measurements are however needed to obtain an in-depth understanding of exchange interactions and of the nature of the magnetic excitations in $Ni_3V_2O_8$.

7.3. Muon studies

Muon-spin relaxation studies have also been used to investigate the local magnetic properties of the ordered phases in a single crystal sample of $Ni_3V_2O_8$ [34]. In the magnetically ordered phases, the muon-spin precession indicates the presence of internal magnetic fields at muon sites in $Ni_3V_2O_8$. The authors find evidence for two distinctly different signals in each of the magnetically ordered phases, which is consistent with different local fields associated with the spine and cross-tie spins. In the LTI phase, having a finite moment on both the spine and cross-tie spins, the μ^+SR signal shows oscillations at two frequencies. In the HTI phase, having long-range order on the spine spins but not on the cross-tie spins, the authors observe an oscillatory component together with a pure relaxation component [34].

8. Modifications of the $Ni_3V_2O_8$ phase diagram

There have been a number of studies probing the effects of perturbations on the ferroelectric and magnetic properties of $Ni_3V_2O_8$. One particularly fruitful set of studies have investigated the effects of hydrostatic pressure [18]. This provides

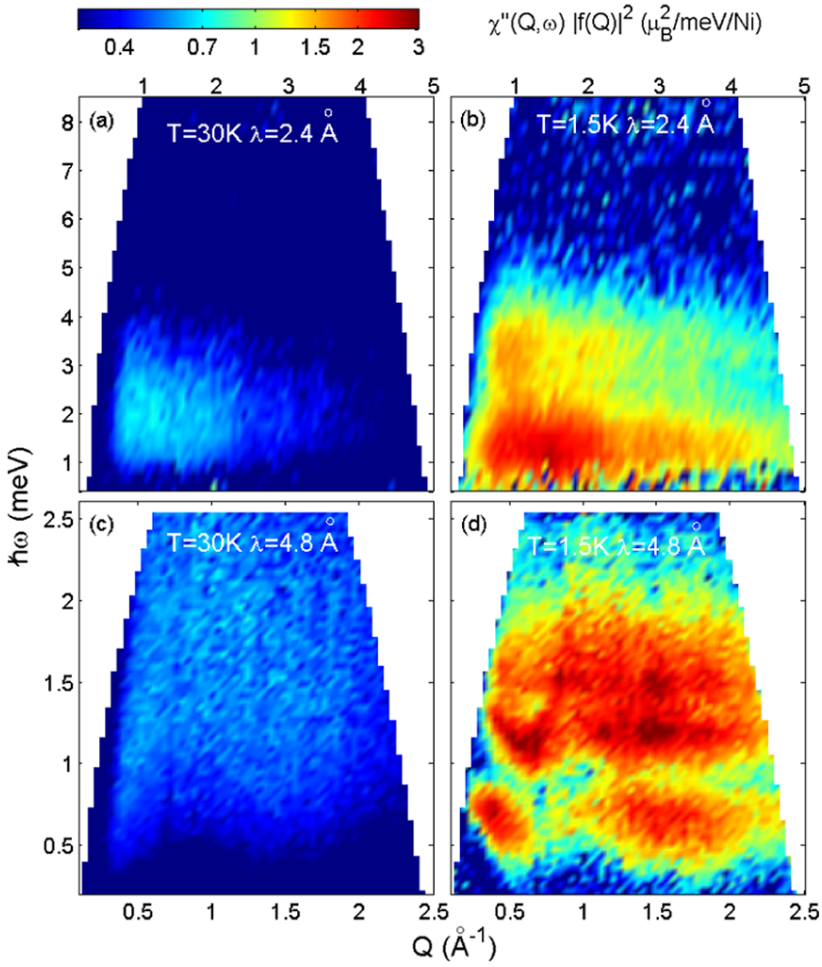

Figure 7. Imaginary part of the dynamic magnetic susceptibility, $\chi''(Q, \hbar\omega)$, as a function of powder averaged wavevector $Q = |\mathbf{Q}|$ and energy transfer $\hbar\omega$, shown for the paramagnetic and commensurate magnetic phase. These data were obtained using the DCS cold-neutron time-of-flight spectrometer at the NIST Center for Neutron Research. The measurements were performed using neutrons with a wavelength of 2.4 Å ((a) and (b)), and 4.8 Å ((c) and (d)), respectively, and were put an absolute scale using the elastic incoherent scattering. The sample weight was approximately 10 g and was cooled in a ^{4}He cryostat.

a method of determining how changing the lattice parameters can promote magnetic structures over others. These measurements found that the multiferroic transition temperature T_L is reduced with applied pressure, with an even larger reduction in the magnitude of the spontaneous electric polarization. A hydrostatic pressure of 1.588 GPa decreases T_L to approximately 6.2 K, while reducing the polarization to less than $P_b \approx 5\ \mu C\ m^{-2}$. While applied pressure reduces T_L it increases T_C, promoting the CAF phase at the expense of the LTI phase. At hydrostatic pressures above 1.64 GPa, the ferroelectric phase is suppressed completely and $Ni_3V_2O_8$ undergoes a direct transition from the HTI phase to the CAF phase [18]. The phase diagram of $Ni_3V_2O_8$ can be modified by a number of other approaches, including Co substitution for Ni [35], and applying an external electric field [36].

9. Conclusion

The detailed materials characterization available for $Ni_3V_2O_8$ allows specific models for multiferroic transitions to be tested quantitatively. Several of the different magnetic phases in $Ni_3V_2O_8$ display striking evidence for strong interactions between spin, lattice, and electric degrees of freedom. These include a significant magnetodielectric coupling, ferroelectricity, strong magneto-optical response, thermal conductivity anomalies, and the pressure dependence of the phase diagram. Despite the large number of studies investigating the properties of $Ni_3V_2O_8$, there remain a number of unanswered questions, including the magnetic structure of C′ phase, and the possible existence of two or more additional magnetic phases at high fields. The magnetic interactions and the nature of the magnetic excitations are also poorly understood in this system. Because of this array of different materials properties, $Ni_3V_2O_8$ is a multi-faceted system for investigating the development of cooperative phenomena in complex oxides. Exploration of this remarkably rich material should help to elucidate the origin of multiferroic behaviors in oxides and inform the search for technologically relevant magnetoelectrics.

Acknowledgments

The authors would like to acknowledge many helpful conversations with A B Harris, A P Ramirez, A Aharony,

J Musfeldt, C Sudakar, R J Cava, P Kharel and T Kimura. We thank Yiming Qiu for help during one of the experiments. Work at Wayne State University was supported by the Institute for Manufacturing Research and the NSF through DMR-0644823. Work at ETH and PSI was supported by the Swiss National Science Foundation under Contract No. PP002-102831. Work at JHU was supported by DMR-0706553. This work utilized facilities supported in part by the National Science Foundation under Agreement No. DMR-0454672.

References

[1] Wolf S A *et al* 2001 *Science* **294** 1488
[2] Spaldin N A and Fiebig M 2005 *Science* **309** 391
[3] Fiebig M 2005 *J. Phys. D: Appl. Phys.* **38** 123
[4] Harris A B and Lawes G 2007 Ferroelectricity in incommensurate magnets *Handbook of Magnetism and Advanced Magnetic Materials* ed H Kronmuller and S Parkin (Chichester: Wiley) pp 2428–60
[5] Zavaliche F *et al* 2007 *Nano Lett.* **7** 1586
[6] Datta S and Das B 1990 *Appl. Phys. Lett.* **56** 665
[7] Fox D L and Scott J F 1977 *J. Phys. C: Solid State Phys.* **10** L329
[8] Fox D L, Tilley D R, Scott J F and Guggenheim H J 1980 *Phys. Rev.* B **21** 2926
[9] Newnham R E, Kramer J J, Schulze W A and Cross L E 1978 *J. Appl. Phys.* **49** 6088
[10] Hill N A 2000 *J. Phys. Chem.* B **104** 6694
[11] Kimura T *et al* 2003 *Nature* **426** 55
[12] Lawes G *et al* 2005 *Phys. Rev. Lett.* **95** 087205
[13] Kenzelmann M *et al* 2005 *Phys. Rev. Lett.* **95** 087206
[14] Wang J *et al* 2003 *Science* **299** 1719
[15] Zheng H *et al* 2004 *Science* **303** 661
[16] Lawes G *et al* 2004 *Phys. Rev. Lett.* **93** 247201
[17] Harris A B, Yildirim T, Aharony A and Entin-Wohlman O 2006 *Phys. Rev.* B **73** 184433
[18] Chaudhury R P, Yen F, dela Cruz C R, Lorenz B, Wang Y Q, Sun Y Y and Chu C W 2007 *Phys. Rev.* B **75** 012407
[19] Balakrishnan G, Petrenko O A, Lees M R and Paul D M K 2004 *J. Phys.: Condens. Matter* **16** L347
[20] Kenzelmann M *et al* 2006 *Phys. Rev.* B **74** 014429
[21] Rai R C *et al* 2006 *Phys. Rev.* B **74** 235101
[22] Wilson N R, Petrenko O A and Balakrishnan G 2007 *J. Phys.: Condens. Matter* **19** 145257
[23] Nagamiya T 1967 *Solid State Phys.* vol 20 , ed F Seitz and D Turnbull (New York: Academic) p 346
[24] Ramirez A P 1994 *Annu. Rev. Mater. Sci.* **24** 453
[25] Rogado N, Lawes G, Huse D A, Ramirez A P and Cava R J 2002 *Solid State Commun.* **124** 229
[26] Jin R, Sha H, Khalifa P G, Sykora R E, Sales B C, Mandrus D and Zhang J 2006 *Phys. Rev.* B **73** 174404
[27] Sharma P A *et al* 2004 *Phys. Rev. Lett.* **93** 177202
[28] Lawes G, Varma C M, Ramirez A P and Subramanian M A 2003 *Phys. Rev.* **91** 257208
[29] Harris A B, Aharony A and Entin-Wohlman O 2008 *Preprint* 0802.0604 [cond-mat]
[30] Lawes G, Kimura T and Ramirez A P 2004 unpublished
[31] Harris A B 2007 *Phys. Rev.* B **76** 054447
[32] Harris A B, Kallin C and Berlinsky A J 1992 *Phys. Rev.* B **45** 2899
[33] Wilson N R *et al* 2007 *J. Magn. Magn. Mater.* **310** 1334
[34] Lancaster T, Blundell S J, Baker P J, Prabhakaran D and Hayes W 2007 *Phys. Rev.* B **75** 064427
[35] Qureshi N *et al* 2006 *Phys. Rev.* B **74** 212407
[36] Kharel P, Sudakar C, Harris A B, Naik R and Lawes G 2007 *Phys. Rev.* B submitted
(Kharel P, Sudakar C, Harris A B, Naik R and Lawes G 2007 *Preprint* 0711.4137 [cond-mat])